

Decoupled Visual Interpretation and Linguistic Reasoning for Math Problem Solving

Zixian Guo^{1,2} Ming Liu¹ Zhilong Ji³ Jinfeng Bai³ Lei Zhang² Wangmeng Zuo^{1,4}

¹Harbin Institute of Technology ²The Hong Kong Polytechnic University ³Tomorrow Advancing Life ⁴Pazhou Lab, Guangzhou

Abstract

Current large vision-language models (LVLMs) typically employ a connector module to link visual features with text embeddings of large language models (LLMs) and use end-to-end training to achieve multi-modal understanding in a unified process. Well alignment needs high-quality pre-training data and a carefully designed training process. Current LVLMs face challenges when addressing complex vision-language reasoning tasks, with their reasoning capabilities notably lagging behind those of LLMs. This paper proposes a paradigm shift: instead of training end-to-end vision-language reasoning models, we advocate for developing a decoupled reasoning framework based on existing visual interpretation specialists and text-based reasoning LLMs. Our approach leverages (1) a dedicated vision-language model to transform the visual content of images into textual descriptions and (2) an LLM to perform reasoning according to the visual-derived text and the original question. This method presents a cost-efficient solution for multi-modal model development by optimizing existing models to work collaboratively, avoiding end-to-end development of vision-language models from scratch. By transforming images into language model-compatible text representations, it facilitates future low-cost and flexible upgrades to upcoming powerful LLMs. We introduce an outcome-rewarded joint-tuning strategy to optimize the cooperation between the visual interpretation and linguistic reasoning model. Evaluation results on vision-language benchmarks demonstrate that the decoupled reasoning framework outperforms recent LVLMs. Our approach yields particularly significant performance gains on visually intensive geometric mathematics problems. The code is available: <https://github.com/guoxiz/DVLR>.

1. Introduction

Recent application of reinforcement techniques to the learning of large language models (LLMs) triggers amazing reasoning ability [21, 28] in the form of long natural language thought or slow-thinking [36]. Much efforts have

been made to extend the powerful reasoning capability to visual and textual multi-modal scenarios [4, 7, 10, 42, 45]. Current development of vision-language models typically employ a connector module, e.g. Linear layers [18], Q-Former [15], Perceiver-Resampler [1], etc., to integrate visual features with text features of LLMs. They collect high-quality image-text paired data and design sophisticated end-to-end training processes to achieve joint visual and textual comprehension and reasoning in a unified process [37, 38].

However, compared to LLMs, existing large vision-language models (LVLMs) can hardly achieve the same level of reasoning proficiency [35, 44]. This gap in performance is particularly evident in visual-intensive tasks that require precise extraction and interpretation of visual information to support complex reasoning processes [12]. We find that a main barrier that hinders effective reasoning is that existing LVLMs struggle with precisely extracting the necessary information from images. The inaccurate understanding of the image brings a bottleneck to the subsequent reasoning process, such as hallucinations in the reasoning steps.

For example, in Figure 1, the foundation model Qwen2VL-7B [32] can not correctly answer the question due to incorrectly associating the variable x with the angle W . However, if we prompt the VL model to describe the figure of the question, it can precisely summarize all the interior angles correctly. Then, we can get the correct answer by using a reasoning LM to derive the solution. We show more similar cases in the supplementary material. Even when the images are frustratingly simple, LVLM can still make obvious mistakes if it answers the question directly. This implies that some parts of the current problems in VL reasoning are not actually reasoning problems but insufficient visual understanding.

This observed discrepancy motivates our thinking of whether an end-to-end visual-language reasoning model is optimal or whether the problem can be more effectively addressed through a division of labor between vision specialists and linguistic reasoners. Current LLMs have reached unprecedented capabilities in textual reasoning [8, 29], while specialized vision models demonstrate remarkable

Directly answer with VL model

Image:

Question: Find $\angle W$. Choices: A:38 B:36 C:76 D:152

Qwen2VL-7B

Solution: Since the sum of the **interior angles of a pentagon is 540**, we have the equation $(x - 8) + (x + 8) + (2x + 7) + (3x - 11) + \angle W = 540$. Solving this equation, we find $\angle W = 152$. Therefore, the answer is D.

Image interpretation with VL model & answer with LM model

Describe the figure. → Qwen2VL-7B

Image description: In pentagon UVWXYZ, it is known that $\angle U = (x - 8)$, $\angle V = (3x - 11)$, $\angle W = (x + 8)$, $\angle Z = (2x + 7)$, and $\angle Y = x$. [Question] The question is that what is the measure of angle W. Find the correct answer from the choices: A:38 B:36 C:76 D:152

→ Qwen2.5Math-7B

Solution: To find the measure of angle $\angle W$ in pentagon UVWXYZ, we start by using the fact that the sum of the **interior angles of a pentagon is 540°**. ... We are given the measures of the angles as follows: $\angle U = (x - 8)^\circ$, $\angle V = (3x - 11)^\circ$, $\angle W = (x + 8)^\circ$, $\angle X = (2x + 7)^\circ$, $\angle Y = x^\circ$. The sum of these angles is equal to 540°. Therefore, we can write the equation: $(x - 8) + (3x - 11) + (x + 8) + (2x + 7) + x = 540$. Next, ... Now that we have the value of x , we can find the measure of angle $\angle W$, which is given by $\angle W = (x + 8)^\circ$ Therefore, the correct answer is: C

Figure 1. Comparison of the solving results of a geometry math problem by directly answering with a VL model or first interpreting the image with a VL model and then answering with an LM model. We can see that the VL model can correctly describe the image even though it can not correctly answer the question. Decoupled reasoning architecture with an image interpreter and a linguistic reasoner can solve the problem correctly.

capabilities in fine-grained image parsing. Rather than pursuing unified training of multi-modal reasoning systems from scratch, it is promising to leverage the complementary strengths of these mature, specialized models to advance visual-language reasoning.

To this end, we propose a decoupled vision-language reasoning architecture that explicitly decouples and orchestrates visual interpretation and linguistic reasoning. Unlike common supervised fine-tuning pipelines, which often train LVLMs to reason and solve problems directly with vision-language input, our method introduces an intermediary step where the LVLM first translates visual content into reasoning context. This translation involves extracting key elements, such as geometric primitives and spatial relationships, into natural language descriptions for the subsequent reasoning phase. The linguistic reasoning is then carried out by an LLM, which processes the natural language conditions aggregated from the input text and image contents to derive the solution through step-by-step reasoning. This specialized division of labor between visual interpretation and linguistic reasoning effectively leverages the complementary strengths of each component.

To achieve an effective collaboration of visual interpretation and linguistic reasoning, we built a three-stage training process for LLMs and LVLMs, with each stage addressing different aspects. In the first stage, we separately tune the LVLMs and LLMs to develop the basic ability to parse images and answer questions, respectively. Based on existing geometric math problem datasets, we built a dataset of ge-

ometric diagrams and interpretation text pairs to train the LVLM to parse images. And we used the solution steps to train the LLM to answer the question. We then connect the LVLM and LLM in series. In the next training stage, we use the correctness of the answer by the LLM as reward feedback to continue optimizing the LVLM, further enabling it to generate more effective image parsing results for LLM reasoning. In the third stage, we fix the LVLM and further tune the LLM to enhance the reasoning performance by rewarding the successful outcome of the response as the reinforced learning objective. This joint tuning strategy ensures both modules collaborate effectively.

Evaluation results on vision-language benchmarks demonstrate that the decoupled framework outperforms recent vision-language models. Our approach yields particularly significant performance gains on visually intensive geometric mathematics problems. In summary, our contributions include:

- We propose a novel decoupled reasoning framework for vision-language reasoning that leverages the strengths of LVLM and LLM for precise image interpretation and linguistic reasoning. We suggest that utilizing the ability of mature specialized models forms a valuable baseline for vision-language reasoning.
- We propose an effective outcome-rewarded joint optimization approach that facilitates the seamless collaboration between the visual interpretation and linguistic reasoning modules.
- Our method demonstrates improvements in vision-

language reasoning tasks, particularly visually intensive geometric math problems. This advancement highlights the effectiveness of the decoupled reasoning architecture.

2. Related Work

2.1. Large Vision-Language Model

The integration of language and visual content has garnered significant attention in recent years, leading to the rapid advancement of large vision-language models (LVLMs). These models aim to bridge the gap between visual and textual modalities, facilitating a more nuanced understanding of multimodal data. Notable methodologies include the Q-former proposed by the BLIP series [14, 15, 17], which utilizes a query-based approach to align visual features with language tokens. Similarly, the LLaVA series [18, 19] and MiniGPT4 [46] leverage the linear layer to enhance the transition between visual and language tokens. The perceiver resampler used by Flamingo [1] also shows effective handling of visual content.

Despite these advancements, achieving a fine-grained joint understanding of visual and linguistic information remains a difficult challenge. Recent models, such as the Qwen-VL series [2, 32], have introduced innovative mechanisms like dynamic visual tokens that adapt to varying image resolutions. There is also work exploring more effective image feature encoding mechanisms [34], which gradually extract more comprehensive visual features from coarse to fine granularity. These enhancements are crucial for improving the accuracy of visual perception and mitigating issues associated with hallucinations, which have historically advanced LVLMs.

2.2. Vision-Language Reasoning

Recently, reinforcement-learning-based fine-tuning [11, 13, 21, 22], test-time scaling [23, 31] and learning from tree search [26, 38, 41] techniques have enabled impressive progress on complex reasoning tasks with large language models [29, 33, 39]. This has inspired people to have a great desire for multimodal joint reasoning of vision and language. However, the interplay between visual perception and reasoning often leads to instability. Fortunately, the increasing availability of high-quality visual-language reasoning datasets [5, 6] has significantly improved the reasoning capabilities of LVLMs.

Geometric math problems, characterized by their visual and linguistic components, have emerged as a focal point for research, as they allow for straightforward verification of results. Various approaches have been proposed, including G-LLaVA [6], Math-LLaVA [30], MultiMath [25], LLaVA-o1 [37], which utilize large language models to expand the diversity of existing datasets by rephrasing and rewriting problems and reasoning steps. InfiMM-WebMath [9] col-

lected a large number of documents containing mathematical knowledge from the Internet. R-COT [5] proposed to synthesize high-quality math reasoning problems by reversely constructing question-answering pairs by prompting LLM with the description of the geometry image. This methodology underscores the effectiveness of supervised fine-tuning with data derived from diverse sources to create capable LVLMs adept at solving graphic mathematical challenges.

Recent efforts to enhance reasoning in large multimodal language models have focused on learning from tree-based exploration [27, 38] and reinforcement learning [16]. For instance, Mulberry [38] proposed a collective-learning-based MCTS framework to explore feasible reasoning paths efficiently and effectively. Learning from the set of well-defined reasoning steps and reflection paths achieves multimodal LLMs with o1-like step-by-step reasoning and reflection capabilities.

As the field continues to evolve, the integration of more effective training methodologies and the development of high-quality datasets will be paramount in advancing the capabilities of LVLMs. Our proposed decoupled reasoning architecture builds upon these foundational works by explicitly decoupling visual interpretation from linguistic reasoning, thereby addressing limitations observed in existing models and paving the way for enhanced performance in complex geometric problem-solving tasks.

3. Method

3.1. Overview

In this section, we introduce how we build the decoupled reasoning vision-language reasoning framework. The training process is divided into three stages. The first stage establishes a robust foundation by supervised fine-tuning of both the LVLM and the LLM. This stage ensures that each module develops the necessary capabilities to perform its designated role effectively. The second stage further reinforces the LVLM to generate informative descriptions of images for the LLM to derive accurate answers. The third stage aims to refine the LLM's ability to reason about the visual information provided by the LVLM and derive accurate solutions through step-by-step reasoning. The overall training pipeline is shown in Figure 2.

3.2. Supervised Fine-tuning of LVLM and LLM

Image Interpretation Dataset. Existing vision-language problem solving datasets [5, 6, 25, 30] are usually in the form of problems and solutions. Problems include images, corresponding questions, and solutions include reasoning steps and final answers. To train the LVLM on the intermediary image interpretation task, we construct a specialized dataset sourced from GeoMM [5]. GeoMM generates

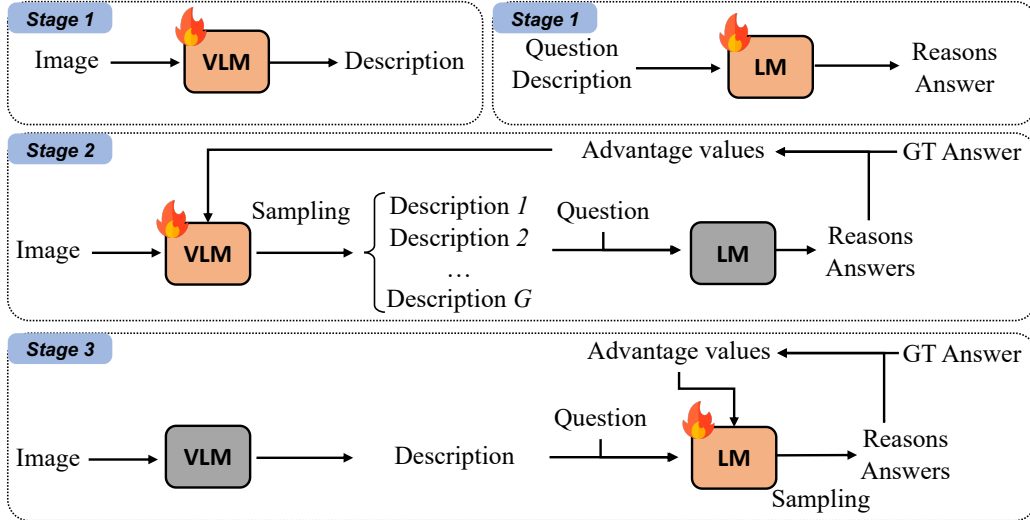


Figure 2. The three-stage model training pipeline of our method. The first supervised fine-tuning stage establishes a foundation of both the LVLM and the LLM. The reinforced training stage two and stage three jointly tune the LVLM and LLM to collaborate to solve the geometry problem.

geometry diagrams by sequential sampling and combining basic shapes. At the same time, it also produces a description of the connection and relation of the shapes as it generates the geometric figure. This description data is used to synthesize questions and answers to fine-tune LVLMs. We believe that the accurate descriptions paired with the images are of great value in training the LVLM to comprehensively understand images.

Although these natural language descriptions contain accurate geometric primitives (e.g., points, lines, angles) and detailed spatial relationships (e.g., parallelism, perpendicularity) present in the diagrams, they are not optimal since they are generated according to rules. These descriptions tend to be long-winded and lack logical order, which leads to suboptimal training results, as shown in Figure 3. To solve this problem, we preprocess the descriptions by prompting GPT-4o to refine the descriptions by removing duplicate contents and improving description order while retaining all relevant visual information.

In addition, in order to deal with the situation where some questions in the visually intensive benchmark test samples are printed in the image, we also augment the images in the dataset. We embed text questions into geometric images and train the model to accurately read the questions and parse the geometric structures in the images. Thanks to the accuracy of the original description and the effective data construction method, we have obtained a high-quality geometric image content parsing dataset.

Learning to Interpret Images. Using the constructed image content interpretation data, we supervise fine-tune the LVLM to conduct two related tasks. The first is to parse

the question text embedded in the image. After reading the question, the second task is to generate a description of the geometric shapes in the image. During testing, the first task is omitted for those testing samples that have provided the question text explicitly. This supervised fine-tuning process equips the LVLM with the basic ability to read the question and identify useful information for solving the question from the image.

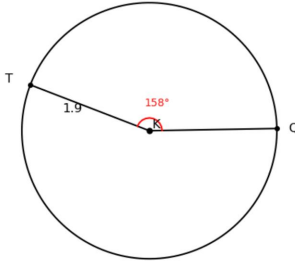
Learning to Reasoning with Visual-Derived Texts. In parallel, we supervise fine-tune the LLM to generate step-by-step solutions depending on the natural language formalized visual conditions. We use the constructed image descriptions and target questions as input and the corresponding solution steps that originate from GeoMM dataset as output to train the LLM, ensuring that the LLM can respond with the desired format (step-by-step reasoning and answer in the end) and logical reasoning steps.

By separating the tasks of visual interpretation and linguistic reasoning, we enable each module to specialize in its respective domain, laying the groundwork for effective collaboration in the subsequent stages of training.

3.3. Reinforced Interpretation Learning of LVLM

After the first training stage, we connect the LVLM and LLM in series. Then, we proceed to the second stage of training, which focuses on reinforcing the LVLM’s ability to generate more informative descriptions of geometric images. This stage employs a reinforcement learning (RL) algorithm, where the correctness of the LLM’s final answer serves as the reward signal for optimizing the LVLM.

Specifically, the LVLM is regarded as the policy model



Description: In the diagram, there is a circle K. There are lines KQ, KT in the diagram. *Point Q lies on the circle K. Point T lies on the circle K. The line KQ is the radius of the circle K. The line KT is the radius of the circle K.* The angle TKQ is the central angle of the circle K. The measure of the angle TKQ is equal to 158 degrees. *The length of the line KT is equal to 1.9.*

↓  GPT-4o
(Prompted by examples)

Description: In circle K, *both KQ and KT are radii. The radius KT is 1.9 units long.*
The angle formed between radii KT and KQ, denoted as $\angle TKQ$, measures 158 degrees.

Figure 3. Demonstration of the geometry image description data. The original image description from the GeoMM dataset is accurate but wordy and lacks logical order. We refined the description to be more concise and logical by prompting GPT-4o.

π_θ . We optimize the policy model by maximizing the objective given by the Group Relative Policy Optimization (GRPO) algorithm [29]:

$$\mathcal{J}_{GRPO}(\theta) = \mathbb{E} \left[q \sim \mathcal{D}, \{o_i\}_{i=1}^G \sim \pi_{\theta_{old}}(O | q) \right] \cdot \\ \frac{1}{G} \sum_{i=1}^G \left(\min \left(\frac{\pi_\theta(o_i | q)}{\pi_{\theta_{old}}(o_i | q)} A_i, \text{clip} \left(\frac{\pi_\theta(o_i | q)}{\pi_{\theta_{old}}(o_i | q)}, 1 - \varepsilon, 1 + \varepsilon \right) A_i \right) - \beta \mathbb{D}_{KL}(\pi_\theta \| \pi_{ref}) \right)$$

where the q denotes the question from training dataset \mathcal{D} , $\{o_i\}_{i=1}^G$ are sampled image description outputs from the LVLM, ε and β are hyper-parameters, and $\{A_i\}_{i=1}^G$ is the advantage values computed by normalizing a group of reward values $\{r_i\}_{i=1}^G$:

$$A_i = \frac{r_i - \text{mean}(r_1, r_2, \dots, r_G)}{\text{std}(r_1, r_2, \dots, r_G)} \quad (2)$$

The KL regular term is formulated as :

$$\mathbb{D}_{KL}(\pi_\theta \| \pi_{ref}) = \frac{\pi_{ref}(o_i | q)}{\pi_\theta(o_i | q)} - \log \frac{\pi_{ref}(o_i | q)}{\pi_\theta(o_i | q)} - 1, \quad (3)$$

In this setup, the LVLM generates several descriptions for the geometric diagram of a training sample. Then, these descriptions, coupled with the text question, are passed to the frozen LLM to solve the problem. The LLM’s outputs, which contain reasoning steps and the final answer in the end, are evaluated against the ground truth answer. In this training stage, we use multiple-choice questions from the Geo170k dataset [6] so that the expected answer is one of the options provided in the question. We extract the final answer from the generated response by regular expressions and then directly compare the generated answer with the

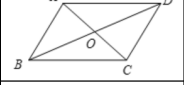
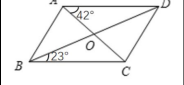
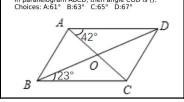
Question Sets	Text Input	Image Input
Text Dominant	Question: In parallelogram ABCD, the diagonal AC and BD intersect at point O, angle DAC = 42.0, angle CBD = 23.0, then angle COD is ().	
Vision Dominant	Question: In parallelogram ABCD, then angle COD is ().	
Vision Only	Question: In ABCD, angle DAC = 42.0, angle CBD = 23.0, then angle COD is ().	

Figure 4. Visualization of different versions of the same problem in MathVerse testmini.

ground truth. A rule-based reward function is used according to the existing method [21]. The reward r_i of the image description o_i is 1 if the comparison of the answer is successful. Otherwise, the reward is set as 0.

To make the optimization effective, we skip the training questions where LM is successful (or unsuccessful) on all the sampled descriptions from LVLM. In other words, if $\{r_i\}_{i=1}^G$ are all equal to 1 or 0, we skip the sample. This reward value design strategy gives feedback to the LVLM, encouraging it to produce descriptions that are more conducive to accurate reasoning by the LLM. This outcome-rewarded tuning strategy ensures that the LVLM learns to prioritize the extraction of visual information that is most relevant for solving the problem.

3.4. Reinforced Reasoning of LLM

In the final stage of training, we aim to stimulate the ability of linguistic reasoning further. We fix the parameters of the LVLM and focus on optimizing the LLM’s reasoning capabilities. We use the same reward-model-free RL framework as the second training stage. However, in this training stage, the outcome-based reward is given to the sampled

Table 1. Comparison of unified vision-language reasoning model LLaVA-CoT and the decoupled reasoning framework.

Model	MMStar	MM-Vet	MathVista	MathVerse
LLaVA-CoT-11B [37]	57.6	60.3	54.8	36.2
Ours-SFT (Init. by Qwen2VL-7B & Qwen2.5Math-7B)	59.1	61.5	57.1	42.5

Table 2. Top-1 Accuracy (%) on geometry math problem solving on the testmini set of MathVerse benchmark.

Model	Text Dominant	Text Lite	Vision Intensive	Vision Dominant	Vision Only
<i>Closed-source Models</i>					
GPT-4o	54.8	52.3	47.3	44.3	43.7
GPT-4o & OpenAI-o1mini	70.6	67.3	64.2	62.0	60.1
<i>Open-source Models</i>					
G-LLaVA-7B [6]	24.9	22.1	18.0	15.2	9.0
Math-LLaVA-13B [30]	22.8	21.8	21.1	19.2	15.4
MultiMath-7B [25]	34.8	30.8	28.1	25.9	15.0
R-CoT-7B [5]	52.3	48.2	42.6	38.5	28.5
Qwen2VL-7B	44.3	41.5	38.2	37.1	33.8
Qwen2VL-72B & Deepseek-V3(671B)	59.1	53.1	48.9	44.2	42.9
Ours (Init. by Qwen2VL-7B & Qwen2.5Math-7B)	54.3	49.0	46.3	47.2	43.8

responses of the LLM policy model. This training stage refines the LLM’s ability to process image interpretations and derive accurate solutions. For the questions that can not be correctly responded to even once in the second train stage, the exploration in the LLM sampling process can discover reasoning paths that lead to correct answers.

Through the joint outcome-rewarded tuning process in stage 2 and stage 3, the LVLM and the LLM can collaborate more effectively, enhancing the overall performance of the decoupled reasoning architecture.

4. Experiment

4.1. Setup

Base model. We conduct experiments with Qwen2VL-7B [32] and Qwen2.5Math-7B as the LVLM and LLM foundation models, respectively. Both of the models are reported to have strong basic capabilities.

Training dataset statistics. GeoMM [5] contains 33344 unique images and 86857 question-answer pairs. Before the supervised fine-tuning process, we embed each question into the corresponding image for augmentation, thus resulting in 86857 pieces of (Image, Question, Description, Solution) data tuple. Geo170k [6] contains 8063 unique images and 117205 question-answer pairs.

Experimental details. Our experiments are done with a set of 4 NVIDIA H20 GPUs. The supervised fine-tuning in the first training stage conducts one epoch for both the LVLM and LLM with 128 batch size and $1e - 4$ learning rate. For the reinforcement learning process in the second

and third training stages, the number of epochs is 5, the batch size is 64, the learning rate is $1e - 6$, and the group number $G = 5$. The hyper-parameters $\varepsilon = 0.2$ and the KL coefficient $\beta = 0.01$.

Benchmarks. We use MMStar [3] and MMVet [40] as the benchmark for evaluating the general visual question-answering capabilities of models. MathVista [20] and MathVerse [43] are used as the benchmark for mathematical reasoning. Compared with the previous mathematical benchmarks, MathVerse is a dataset designed to assess the performance of LVLMs in strongly visual-dependent situations. It contains test cases with strong visual dependencies in order to truly verify the LVLM’s ability to understand images. As shown in Figure 4, it constructs five different ways of asking for the same question. From the “Text Dominant” set to the “Vision Only” set, the input becomes more and more visually dependent and requires a higher ability of visual understanding. We use regular expression to extract the final answer from the output response of the model and compare the answer with the ground truth to determine the correctness of the result.

4.2. Effectiveness of Decoupled Reasoning

To demonstrate the advantages of the decoupled reasoning method, we compare it with the recent end-to-end vision-language model LLaVA-CoT [37]. With carefully organized data, LLaVA-CoT trains the VLM to independently carry out sequential stages of four sub-tasks: summarization, visual interpretation, logical reasoning, and conclusion generation. To build the decoupled inference pipeline

accordingly, we divide the output of the training data of LLaVA-CoT into two parts. The summarization and visual interpretation are used to supervise the dedicated VLM to analyze the question and describe the image. The logical reasoning and conclusion content are used to train the LLM.

After supervise fine-tuning the VLM for visual interpretation and LLM for linguistic reasoning separately, we evaluate the result. From Table 1, we can see that the decoupled reasoning method outperforms LLaVA-CoT in general visual question-answering and math vision problems. This shows the rationality of building cross-modal reasoning models based on the advantages of existing mature, specialized models.

4.3. Effectiveness of Joint-Tuning for Decoupled Reasoning

Compared methods. To fully verify the effectiveness of our method, we selected a variety of comparison methods as strong opponents, as shown in Table 2. We compared the current top-performing closed-source models and open-source models and tried two testing strategies: directly using LVLM to answer questions and using LVLM to interpret images and then using LLM to infer and solve questions. Specifically, we use GPT-4o (version “gpt-4o-2024-11-20”) [24] as the closed-source LVLM model, GPT-4o & OpenAI-o1mini (version “o1-mini-2024-09-12”) as the closed-source LVLM + LLM setting, Qwen2VL-7B as the open-source general LVLM model, R-CoT-7B [5] as the open-source geometry-specific LVLM model, Qwen2VL-72B & Deepseek-V3(671B) as the open-source LVLM + LLM setting.

For these compared methods, the test setting of lonely LVLM is zero-shot prompting, i.e., we directly instruct the LVLM to think and finally answer the question according to the image. For the LVLM interpretation and LLM reasoning inference pipeline, we prompt LVLM with one in-context example because we found that prompting with an example can demonstrate the image interpretation task to LVLM better and make the output format of LVLM more stable. For the linguistic reasoner LLM, we use zero-shot instruction. For our methods, after we train the LVLM and LLM in three training stages, we use zero-shot prompting for both the LVLM and LLM. The details of the adopted prompts can be found in the supplementary material.

From Table 2, “GPT-4o & OpenAI-o1mini” serves as the closed-source SOTA method surpassing “GPT-4o” by a large margin, demonstrating that the decoupled reasoning pipeline bears significant effectiveness in solving geometry math problems. “Qwen2VL-72B & Deepseek-V3(671B)” accordingly demonstrates the effectiveness of open-source models. The open-source geometry-specific LVLM model, R-CoT-7B, has a competitive performance in “Text Dominant” and “Text Lite” sets of the benchmark. However,

Table 3. Ablation study of image description preprocessing (denoted as $P(\cdot)$).

Test Sets	w/o $P(\cdot)$	w $P(\cdot)$
Text Dominant	47.9	52.3
Text Lite	42.6	46.9
Vision Intensive	39.5	42.2
Vision Dominant	38.8	42.6
Vision Only	36.7	39.7

Table 4. Ablation study of decoupled reasoning and LVLM only.

Test Sets	LVLM Only	Ours
Text Dominant	51.1	54.3
Text Lite	46.5	49.0
Vision Intensive	41.5	46.3
Vision Dominant	39.1	47.2
Vision Only	37.3	43.8

Table 5. Ablation study of the training stages.

Stage1(SFT)	✓	✓	✓	✓
Stage2(RL-VLM)	✗	✓	✗	✓
Stage3(RL-LM)	✗	✗	✓	✓
Text Dominant	52.3	51.5	53.2	54.3
Text Lite	46.9	47.3	49.8	49.0
Vision Intensive	42.2	44.7	45.2	46.3
Vision Dominant	42.6	45.5	44.1	47.2
Vision Only	39.7	42.8	40.6	43.8

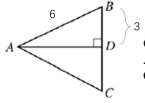
its performance drops significantly (e.g., “Vision Only” –23.8) when vision information becomes harder to extract.

Compared to these opponents, our trained model, which is initialized from “Qwen2VL-7B & Qwen2.5Math-7B”, demonstrates advantages, especially in the “Vision Dominant” and “Vision Only” sets. Equipped with decoupled reasoning architecture, our method can interpret and better understand geometry images with more important conditions related to solving the question. Our method is close to the top-performing open-source method “Qwen2VL-72B & Deepseek-V3(671B)”, whose model size is dozens of times larger than ours. The results demonstrate the effectiveness of our decoupled reasoning framework that combines visual interpretation and linguistic reasoning for better geometry problem-solving.

4.4. Ablation Study

To further validate the effectiveness of our method, we conduct an ablation study to examine the contribution of each component. We evaluate the performance of the model with the following settings varied:

Effectiveness of image description preprocessing. We ablate the effectiveness of preprocessing the image description



Question: In triangle ABC above, the bisector of angle BAC is AD. The length of AB is equal to the length of AC. What is the measure of angle BAC?
Choices: A:15 B:30 C:45 D:60 E:75

VLM (Stage1):

The given problem involves a triangle ABC with the bisector of angle BAC being AD. The length of AB is equal to the length of AC. The question asks for the measure of angle BAC. The provided image **shows the triangle with the given lengths** and the bisector AD. The multiple-choice options

LLM:

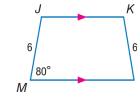
Given that triangle ABC is isosceles with $AB = AC$ and AD is the angle bisector of $\angle BAC$, we need to determine the measure of $\angle BAC$. Since $AB = AC$, triangle ABC is isosceles, and the base angles $\angle ABC$ and $\angle ACB$ are equal. Let's denote the measure of $\angle BAC$ by $2x$. Therefore, the measure of each base angle is $90^\circ - x$. The angle bisector AD divides $\angle BAC$ into two equal angles, so $\angle BAD = \angle CAD = x$. Now, let's consider the sum of the angles in triangle ABC: $\angle BAC + \angle ABC + \angle ACB = 180^\circ$. Substituting the values we have: $\angle BAC + 2(90^\circ - x) = 180^\circ$. Simplifying the left side: $2x + 180^\circ - 2x = 180^\circ$. This equation is always true, but it doesn't give us the value of x directly.

VLM (Stage2):

In triangle ABC, it is known that $AB = AC$, AD is the bisector of angle BAC. **The length of AB is 6, and the length of BD is 3.** The question is that what is the measure of angle BAC. Find the

LLM:

To determine the measure of angle BAC in triangle ABC, we start by noting that triangle ABC is isosceles with $AB = AC$. This means that angles ABC and ACB are equal. AD divides angle BAC into two equal angles, so $\angle BAD = \angle CAD$. This also means that **triangle ABD and triangle ACD are congruent** by the Angle-Side-Angle (ASA) congruence criterion. This implies $BD = DC$. Given that $BD = 3$, so DC is also 3. Therefore, the entire length of BC is $BD + DC = 3 + 3 = 6$. **This means triangle ABC is not just isosceles but equilateral, since all sides are equal.** Therefore, $\angle BAC = 60^\circ$.



Question: JK is parallel to ML. Find m \angle K. Choices: A:6 B:60 C:100 D:180

VLM (Stage1):

The given problem is a geometry problem involving a **parallelogram**. The known conditions are:
- The **parallelogram** has sides JK and ML, with JK parallel to ML.
- The length of JM and KL is 6 units.
- The angle between JM and ML is 80 degrees.

LLM:

To find the measure of angle K in the given parallelogram, we start by recalling a **key property of parallelograms: opposite angles are equal, and consecutive angles are supplementary (they add up to 180 degrees)**. Given: JK || parallel ML - JM = KL = 6 units - The angle between JM and ML is 80 degrees. Since JK || parallel ML, the angle between JM and ML is the same as the angle between JK and the adjacent side KL. In a parallelogram, consecutive angles are supplementary. **Therefore, angle J and angle L are each 100 degrees. And angle K and angle J add up to 180 degrees.** Since angle J is 100 degrees, we can find angle K as follows: $\angle K = 180^\circ - \angle J = 180^\circ - 100^\circ = 80^\circ$. Thus, the measure of angle K is $\boxed{80}$.

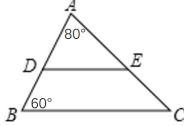
VLM (Stage2):

In quadrilateral JKLM, it is known that JK is parallel to ML, and angle M = 80.0. The question is that what is the measure of angle K. Find the correct answer from the choices:

LLM:

To determine the measure of angle K in quadrilateral JKLM where JK is parallel to ML and angle J is 80 degrees, we can use the properties of a trapezoid. Since JK is parallel to ML, **quadrilateral JKLM is a trapezoid**. In a trapezoid, the consecutive interior angles along the same leg are supplementary, meaning they add up to 180 degrees. Since angle L and angle K are consecutive interior angles, we can write the equation: $\angle L + \angle K = 180^\circ$. Substituting the value of angle L into the equation, we get: $\angle L + \angle K = 180^\circ$. **To find angle K, we subtract 80 degrees from both sides of the equation:** $\angle K = 180^\circ - 80^\circ = 100^\circ$. Therefore, the measure of angle K is $\boxed{100}$.

Figure 5. The output examples of decoupled vision-language reasoning method. The left example shows that reinforced finetuning can enhance the detail of the generated description (i.e., the exact length of the segment). The right example shows that it can improve the description accuracy (parallelogram v.s. quadrilateral).



Question: As shown in the figure, DE parallel BC, then the size of angle CED is ()
Choices: A:40 B:60 C:120 D:140

Describe in detail the composition of the geometric shapes in the image.

VLM (SFT data without $P(\cdot)$): There is a triangle in the diagram, represented by the symbol BAC. Point D lies on line BA. Point E lies on line AC. **Point I lies on line CB.** The measure of angle CBA is equal to 60 degrees. **The length of line CB is 1.** ...

VLM (SFT data with $P(\cdot)$): There is a triangle ABC with DE parallel to BC. The measure of angle CBA is 60 degrees, and the measure of angle BAC is 80 degrees. The question is to determine the measure of angle CED. The options provided ...

Figure 6. Image interpretation result of the LVLM if preprocessing is not performed.

data in the SFT stage of VLM. The original image descriptions of the GeoMM images are generated by predefined rules, which contain a large number of parallel sentences, like "*Point {} lies on line {}.*", and "*The length of line {} is {}.*". This kind of expression, without proper logical order, can easily make the trained VLM generate hallucinatory content with the same sentence structure, as shown in Figure 6. Besides, the overly verbose and chaotically ordered descriptions may make it more difficult for the LLM to process useful conditions for reasoning. From Table 3, we can see that preprocessing the original image descriptions from GeoMM has a positive effect on the results of the supervised fine-tuning stage.

Decoupled Reasoning or LVLM-only. For comparison, we conduct the LVLM-only experiment by supervised fine-tuning using the GeoMM dataset based on the Qwen2VL-7B model. Augmented GeoMM images (according to Section 2.2) are used as input and the reasoning steps of the questions are used as output. After supervised fine-tuning, we then perform reinforcement learning using the Geo170k dataset. During reinforcement learning, the LVLM is tuned by the same outcome-rewarding strategy as Section 2.4. The results in Table 4 show the advantages of our decoupled reasoning method over a single LVLM.

Although a single large model that can jointly understand both vision and language input is desirable, we believe that current small-scale LVLMs still have difficulty balancing the exploration capability required for reasoning and the stability required for precise image understanding. Although straightforward, our decoupled reasoning strategy effectively leverages the strengths of explicit visual interpretation and linguistic reasoning, enabling more nuanced understanding and contextual awareness.

Effectiveness of training stages. The results in Table 5 examine the effectiveness of each training stage. According to the results, both supervised fine-tuning and reinforcement learning of LVLM on image interpretation lead to clear improvements in the visually dependent test cases. As shown in Figure 5, supervised fine-tuning enables VLM to interpret images, but it may still miss some details or generate incorrect comprehension. After the second stage of training, VLM can improve the completeness and accuracy of image information extraction. Performing a complete three-stage

joint tuning can further improve and achieve the best results. This confirms the importance of both the visual interpretation and linguistic reasoning modules, as well as the proper collaboration achieved by joint tuning.

5. Conclusion

This paper introduces a decoupled vision-language reasoning framework that divides the vision-language problem into visual interpretation and linguistic reasoning. Visual interpretation specialized VLMs and linguistic reasoning specialized LLMs are optimized to work collaboratively, avoiding end-to-end training of a vision-language model from scratch. This method presents a cost-efficient solution for multimodal model development. By transforming images into language model-compatible text representations, it facilitates future low-cost and flexible upgrades to upcoming powerful LLMs. Our findings suggest that this framework, preserving the distinct strengths of mature, specialized visual understanding and language reasoning models, forms a valuable baseline for vision-language reasoning. Experimental results demonstrate significant improvements in performance on visually intensive geometric math problems, particularly in tasks requiring robust visual understanding. We anticipate that future work will extend this framework to develop VL reasoning capabilities further, enabling a more comprehensive understanding of visual and linguistic information.

6. Limitations

At present, the joint tuning of the decoupled reasoning framework has been verified in math problems. When faced with more diverse graphic reasoning problems, it may be necessary to introduce more diverse data to enable VLM to interpret the content comprehensively.

References

- [1] Jean-Baptiste Alayrac, Jeff Donahue, Pauline Luc, Antoine Miech, Iain Barr, Yana Hasson, Karel Lenc, Arthur Mensch, Katherine Millican, Malcolm Reynolds, et al. Flamingo: a visual language model for few-shot learning. *Advances in neural information processing systems*, 35:23716–23736, 2022. [1](#), [3](#)
- [2] Jinze Bai, Shuai Bai, Yunfei Chu, Zeyu Cui, Kai Dang, Xiaodong Deng, Yang Fan, Wenbin Ge, Yu Han, Fei Huang, et al. Qwen technical report. *arXiv preprint arXiv:2309.16609*, 2023. [3](#)
- [3] Lin Chen, Jinsong Li, Xiaoyi Dong, Pan Zhang, Yuhang Zang, Zehui Chen, Haodong Duan, Jiaqi Wang, Yu Qiao, Dahua Lin, et al. Are we on the right way for evaluating large vision-language models? *arXiv preprint arXiv:2403.20330*, 2024. [6](#)
- [4] Zihui Cheng, Qiguang Chen, Jin Zhang, Hao Fei, Xiaocheng Feng, Wanxiang Che, Min Li, and Libo Qin. Comt: A novel benchmark for chain of multi-modal thought on large vision-language models, 2024. [1](#)
- [5] Linger Deng, Yuliang Liu, Bohan Li, Dongliang Luo, Liang Wu, Chengquan Zhang, Pengyuan Lyu, Ziyang Zhang, Gang Zhang, Errui Ding, Yingying Zhu, and Xiang Bai. R-cot: Reverse chain-of-thought problem generation for geometric reasoning in large multimodal models, 2024. [3](#), [6](#), [7](#)
- [6] Jiahui Gao, Renjie Pi, Jipeng Zhang, Jiacheng Ye, Wanjun Zhong, Yufei Wang, Lanqing Hong, Jianhua Han, Hang Xu, Zhenguo Li, and Lingpeng Kong. G-llava: Solving geometric problem with multi-modal large language model, 2023. [3](#), [5](#), [6](#)
- [7] Jun Gao, Yongqi Li, Ziqiang Cao, and Wenjie Li. Interleaved-modal chain-of-thought, 2024. [1](#)
- [8] Daya Guo, Dejian Yang, Haowei Zhang, Junxiao Song, Ruoyu Zhang, Runxin Xu, Qihao Zhu, Shirong Ma, Peiyi Wang, Xiao Bi, et al. Deepseek-r1: Incentivizing reasoning capability in llms via reinforcement learning. *arXiv preprint arXiv:2501.12948*, 2025. [1](#)
- [9] Xiaotian Han, Yiren Jian, Xuefeng Hu, Haogeng Liu, Yiqi Wang, Qihang Fan, Yuang Ai, Huibo Huang, Ran He, Zhenheng Yang, and Quanzeng You. Infimm-webmath-40b: Advancing multimodal pre-training for enhanced mathematical reasoning, 2024. [3](#)
- [10] Yunzhuo Hao, Jiawei Gu, Huichen Will Wang, Linjie Li, Zhengyuan Yang, Lijuan Wang, and Yu Cheng. Can mllms reason in multimodality? emma: An enhanced multimodal reasoning benchmark, 2025. [1](#)
- [11] Arian Hosseini, Xingdi Yuan, Nikolay Malkin, Aaron Courville, Alessandro Sordoni, and Rishabh Agarwal. V-star: Training verifiers for self-taught reasoners, 2024. [3](#)
- [12] Kung-Hsiang Huang, Can Qin, Haoyi Qiu, Philippe Laban, Shafiq Joty, Caiming Xiong, and Chien-Sheng Wu. Why vision language models struggle with visual arithmetic? towards enhanced chart and geometry understanding, 2025. [1](#)
- [13] Aviral Kumar, Vincent Zhuang, Rishabh Agarwal, Yi Su, John D. Co-Reyes, Avi Singh, Kate Baumli, Shariq Iqbal, Colton Bishop, Rebecca Roelofs, Lei M. Zhang, Kay McKinney, Disha Shrivastava, Cosmin Paduraru, George Tucker,

Doina Precup, Feryal Behbahani, and Aleksandra Faust. Training language models to self-correct via reinforcement learning, 2024. [3](#)

[14] Junnan Li, Dongxu Li, Caiming Xiong, and Steven Hoi. Blip: Bootstrapping language-image pre-training for unified vision-language understanding and generation. In *International conference on machine learning*, pages 12888–12900. PMLR, 2022. [3](#)

[15] Junnan Li, Dongxu Li, Silvio Savarese, and Steven Hoi. Blip-2: Bootstrapping language-image pre-training with frozen image encoders and large language models. In *International conference on machine learning*, pages 19730–19742. PMLR, 2023. [1, 3](#)

[16] Hunter Lightman, Vineet Kosaraju, Yura Burda, Harri Edwards, Bowen Baker, Teddy Lee, Jan Leike, John Schulman, Ilya Sutskever, and Karl Cobbe. Let’s verify step by step, 2023. [3](#)

[17] Haotian Liu, Chunyuan Li, Qingyang Wu, and Yong Jae Lee. Visual instruction tuning. *Advances in neural information processing systems*, 36:34892–34916, 2023. [3](#)

[18] Haotian Liu, Chunyuan Li, Qingyang Wu, and Yong Jae Lee. Visual instruction tuning. *Advances in neural information processing systems*, 36:34892–34916, 2023. [1, 3](#)

[19] Haotian Liu, Chunyuan Li, Yuheng Li, and Yong Jae Lee. Improved baselines with visual instruction tuning. In *Proceedings of the IEEE/CVF Conference on Computer Vision and Pattern Recognition*, pages 26296–26306, 2024. [3](#)

[20] Pan Lu, Hritik Bansal, Tony Xia, Jiacheng Liu, Chunyuan Li, Hannaneh Hajishirzi, Hao Cheng, Kai-Wei Chang, Michel Galley, and Jianfeng Gao. Mathvista: Evaluating mathematical reasoning of foundation models in visual contexts, 2024. [6](#)

[21] Trung Quoc Luong, Xinbo Zhang, Zhanming Jie, Peng Sun, Xiaoran Jin, and Hang Li. Reft: Reasoning with reinforced fine-tuning, 2024. [1, 3, 5](#)

[22] Chengqi Lyu, Songyang Gao, Yuzhe Gu, Wenwei Zhang, Jianfei Gao, Kuikun Liu, Ziyi Wang, Shuaibin Li, Qian Zhao, Haian Huang, Weihan Cao, Jiangning Liu, Hongwei Liu, Junnan Liu, Songyang Zhang, Daha Lin, and Kai Chen. Exploring the limit of outcome reward for learning mathematical reasoning, 2025. [3](#)

[23] Niklas Muennighoff, Zitong Yang, Weijia Shi, Xiang Lisa Li, Li Fei-Fei, Hannaneh Hajishirzi, Luke Zettlemoyer, Percy Liang, Emmanuel Candès, and Tatsunori Hashimoto. S1: Simple test-time scaling, 2025. [3](#)

[24] OpenAI, Josh Achiam, Steven Adler, Sandhini Agarwal, Lama Ahmad, Ilge Akkaya, Florencia Leoni Aleman, Diogo Almeida, Janko Altenschmidt, Sam Altman, Shyamal Anadkat, Red Avila, Igor Babuschkin, Suchir Balaji, Valerie Balcom, Paul Baltescu, Haiming Bao, Mohammad Bavarian, Jeff Belgum, Irwan Bello, Jake Berdine, Gabriel Bernadett-Shapiro, Christopher Berner, Lenny Bogdonoff, Oleg Boiko, Madelaine Boyd, Anna-Luisa Brakman, Greg Brockman, Tim Brooks, Miles Brundage, Kevin Button, Trevor Cai, Rosie Campbell, Andrew Cann, Brittany Carey, Chelsea Carlson, Rory Carmichael, Brooke Chan, Che Chang, Fotis Chantzis, Derek Chen, Sully Chen, Ruby Chen, Jason Chen, Mark Chen, Ben Chess, Chester Cho, Casey Chu, Hyung Won Chung, Dave Cummings, Jeremiah Currier, Yunxing Dai, Cory Decareaux, Thomas Degry, Noah Deutsch, Damien Deville, Arka Dhar, David Dohan, Steve Dowling, Sheila Dunning, Adrien Ecoffet, Atty Eleti, Tyna Eloundou, David Farhi, Liam Fedus, Niko Felix, Simón Posada Fishman, Juston Forte, Isabella Fulford, Leo Gao, Elie Georges, Christian Gibson, Vik Goel, Tarun Gognani, Gabriel Goh, Rapha Gontijo-Lopes, Jonathan Gordon, Morgan Grafstein, Scott Gray, Ryan Greene, Joshua Gross, Shixiang Shane Gu, Yufei Guo, Chris Hallacy, Jesse Han, Jeff Harris, Yuchen He, Mike Heaton, Johannes Heidecke, Chris Hesse, Alan Hickey, Wade Hickey, Peter Hoeschele, Brandon Houghton, Kenny Hsu, Shengli Hu, Xin Hu, Joost Huizinga, Shantanu Jain, Shawn Jain, Joanne Jang, Angela Jiang, Roger Jiang, Haozhun Jin, Denny Jin, Shino Jomoto, Billie Jonn, Heewoo Jun, Tomer Kaftan, Łukasz Kaiser, Ali Kamali, Ingmar Kanitscheider, Nitish Shirish Keskar, Tabarak Khan, Logan Kilpatrick, Jong Wook Kim, Christina Kim, Yongjik Kim, Jan Hendrik Kirchner, Jamie Kiros, Matt Knight, Daniel Kokotajlo, Łukasz Kondraciuk, Andrew Kondrich, Aris Konstantinidis, Kyle Kosic, Gretchen Krueger, Vishal Kuo, Michael Lampe, Ikai Lan, Teddy Lee, Jan Leike, Jade Leung, Daniel Levy, Chak Ming Li, Rachel Lim, Molly Lin, Stephanie Lin, Mateusz Litwin, Theresa Lopez, Ryan Lowe, Patricia Lue, Anna Makanju, Kim Malfacini, Sam Manning, Todor Markov, Yaniv Markovski, Bianca Martin, Katie Mayer, Andrew Mayne, Bob McGrew, Scott Mayer McKinney, Christine McLeavey, Paul McMillan, Jake McNeil, David Medina, Aalok Mehta, Jacob Menick, Luke Metz, Andrey Mishchenko, Pamela Mishkin, Vinnie Monaco, Evan Morikawa, Daniel Mossing, Tong Mu, Mira Murati, Oleg Murk, David Mély, Ashvin Nair, Rei-ichi Nakano, Rajeev Nayak, Arvind Neelakantan, Richard Ngo, Hyeonwoo Noh, Long Ouyang, Cullen O’Keefe, Jakub Pachocki, Alex Paino, Joe Palermo, Ashley Pantuliano, Giambattista Parascandolo, Joel Parish, Emy Parparita, Alex Passos, Mikhail Pavlov, Andrew Peng, Adam Perelman, Filipe de Avila Belbute Peres, Michael Petrov, Henrique Ponde de Oliveira Pinto, Michael, Pokorny, Michelle Pokrass, Vitchyr H. Pong, Tolly Powell, Alethea Power, Boris Power, Elizabeth Proehl, Raul Puri, Alec Radford, Jack Rae, Aditya Ramesh, Cameron Raymond, Francis Real, Kendra Rimbach, Carl Ross, Bob Rotstetd, Henri Roussez, Nick Ryder, Mario Saltarelli, Ted Sanders, Shibani Santurkar, Girish Sastry, Heather Schmidt, David Schnurr, John Schulman, Daniel Selsam, Kyla Sheppard, Toki Sherbakov, Jessica Shieh, Sarah Shoker, Pranav Shyam, Szymon Sidor, Eric Sigler, Maddie Simens, Jordan Sitkin, Katarina Slama, Ian Sohl, Benjamin Sokolowsky, Yang Song, Natalie Staudacher, Felipe Petroski Such, Natalie Summers, Ilya Sutskever, Jie Tang, Nikolas Tezak, Madeleine B. Thompson, Phil Tillett, Amin Tootoonchian, Elizabeth Tseng, Preston Tuggle, Nick Turley, Jerry Tworek, Juan Felipe Cerón Uribe, Andrea Valalone, Arun Vijayvergiya, Chelsea Voss, Carroll Wainwright, Justin Jay Wang, Alvin Wang, Ben Wang, Jonathan Ward, Jason Wei, C. J. Weinmann, Akila Welihinda, Peter Weller, Jiayi Weng, Lilian Weng, Matt Wiethoff, Dave Willner, Clemens Winter, Samuel Wolrich, Hannah Wong, Lauren

Workman, Sherwin Wu, Jeff Wu, Michael Wu, Kai Xiao, Tao Xu, Sarah Yoo, Kevin Yu, Qiming Yuan, Wojciech Zaremba, Rowan Zellers, Chong Zhang, Marvin Zhang, Shengjia Zhao, Tianhao Zheng, Juntang Zhuang, William Zhuk, and Barret Zoph. Gpt-4 technical report, 2024. 7

[25] Shuai Peng, Di Fu, Liangcai Gao, Xiuqin Zhong, Hongguang Fu, and Zhi Tang. Multimath: Bridging visual and mathematical reasoning for large language models, 2024. 3, 6

[26] Zhenting Qi, Mingyuan Ma, Jiahang Xu, Li Lyra Zhang, Fan Yang, and Mao Yang. Mutual reasoning makes smaller llms stronger problem-solvers, 2024. 3

[27] Yiwei Qin, Xuefeng Li, Haoyang Zou, Yixiu Liu, Shijie Xia, Zhen Huang, Yixin Ye, Weizhe Yuan, Hector Liu, Yuanzhi Li, and Pengfei Liu. O1 replication journey: A strategic progress report – part 1, 2024. 3

[28] Rafael Rafailev, Archit Sharma, Eric Mitchell, Christopher D Manning, Stefano Ermon, and Chelsea Finn. Direct preference optimization: Your language model is secretly a reward model. *Advances in Neural Information Processing Systems*, 36:53728–53741, 2023. 1

[29] Zhihong Shao, Peiyi Wang, Qihao Zhu, Runxin Xu, Junxiao Song, Xiao Bi, Haowei Zhang, Mingchuan Zhang, YK Li, Y Wu, et al. Deepseekmath: Pushing the limits of mathematical reasoning in open language models. *arXiv preprint arXiv:2402.03300*, 2024. 1, 3, 5

[30] Wenhao Shi, Zhiqiang Hu, Yi Bin, Junhua Liu, Yang Yang, See-Kiong Ng, Lidong Bing, and Roy Ka-Wei Lee. Math-llava: Bootstrapping mathematical reasoning for multimodal large language models, 2024. 3, 6

[31] Charlie Snell, Jaehoon Lee, Kelvin Xu, and Aviral Kumar. Scaling llm test-time compute optimally can be more effective than scaling model parameters, 2024. 3

[32] Peng Wang, Shuai Bai, Sinan Tan, Shijie Wang, Zhihao Fan, Jinze Bai, Keqin Chen, Xuejing Liu, Jialin Wang, Wenbin Ge, et al. Qwen2-vl: Enhancing vision-language model’s perception of the world at any resolution. *arXiv preprint arXiv:2409.12191*, 2024. 1, 3, 6

[33] Peiyi Wang, Lei Li, Zhihong Shao, R. X. Xu, Damai Dai, Yifei Li, Deli Chen, Y. Wu, and Zhifang Sui. Math-shepherd: Verify and reinforce llms step-by-step without human annotations, 2024. 3

[34] Haoran Wei, Youyang Yin, Yumeng Li, Jia Wang, Liang Zhao, Jianjian Sun, Zheng Ge, and Xiangyu Zhang. Slow perception: Let’s perceive geometric figures step-by-step, 2024. 3

[35] Yifan Wu, Pengchuan Zhang, Wenhan Xiong, Barlas Ogun, James C. Gee, and Yixin Nie. The role of chain-of-thought in complex vision-language reasoning task, 2023. 1

[36] Kun Xiang, Zhili Liu, Zihao Jiang, Yunshuang Nie, Runhui Huang, Haoxiang Fan, Hanhui Li, Weiran Huang, Yihan Zeng, Jianhua Han, Lanqing Hong, Hang Xu, and Xiaodan Liang. Atomthink: A slow thinking framework for multimodal mathematical reasoning, 2024. 1

[37] Guowei Xu, Peng Jin, Li Hao, Yibing Song, Lichao Sun, and Li Yuan. Llava-o1: Let vision language models reason step-by-step, 2024. 1, 3, 6

[38] Huanjin Yao, Jiaxing Huang, Wenhao Wu, Jingyi Zhang, Yibo Wang, Shunyu Liu, Yingjie Wang, Yuxin Song, Haocheng Feng, Li Shen, and Dacheng Tao. Mulberry: Empowering mllm with o1-like reasoning and reflection via collective monte carlo tree search, 2024. 1, 3

[39] Longhui Yu, Weisen Jiang, Han Shi, Jincheng Yu, Zhengying Liu, Yu Zhang, James T Kwok, Zhenguo Li, Adrian Weller, and Weiyang Liu. Metamath: Bootstrap your own mathematical questions for large language models. *arXiv preprint arXiv:2309.12284*, 2023. 3

[40] Weihao Yu, Zhengyuan Yang, Linjie Li, Jianfeng Wang, Kevin Lin, Zicheng Liu, Xinchao Wang, and Lijuan Wang. Mm-vet: Evaluating large multimodal models for integrated capabilities. *arXiv preprint arXiv:2308.02490*, 2023. 6

[41] Di Zhang, Jianbo Wu, Jingdi Lei, Tong Che, Jiatong Li, Tong Xie, Xiaoshui Huang, Shufei Zhang, Marco Pavone, Yuqiang Li, Wanli Ouyang, and Dongzhan Zhou. Llama-berry: Pairwise optimization for o1-like olympiad-level mathematical reasoning, 2024. 3

[42] Jiarui Zhang, Ollie Liu, Tianyu Yu, Jinyi Hu, and Willie Neiswanger. Euclid: Supercharging multimodal llms with synthetic high-fidelity visual descriptions, 2024. 1

[43] Renrui Zhang, Dongzhi Jiang, Yichi Zhang, Haokun Lin, Ziyu Guo, Pengshuo Qiu, Aojun Zhou, Pan Lu, Kai-Wei Chang, Peng Gao, and Hongsheng Li. Mathverse: Does your multi-modal llm truly see the diagrams in visual math problems?, 2024. 6

[44] Ruohong Zhang, Bowen Zhang, Yanghao Li, Haotian Zhang, Zhiqing Sun, Zhe Gan, Yinfei Yang, Ruoming Pang, and Yiming Yang. Improve vision language model chain-of-thought reasoning. *arXiv preprint arXiv:2410.16198*, 2024. 1

[45] Yizhe Zhang, He Bai, Ruixiang Zhang, Jiatao Gu, Shuangfei Zhai, Josh Susskind, and Navdeep Jaitly. How far are we from intelligent visual deductive reasoning?, 2024. 1

[46] Deyao Zhu, Jun Chen, Xiaoqian Shen, Xiang Li, and Mohamed Elhoseiny. Minigpt-4: Enhancing vision-language understanding with advanced large language models. *arXiv preprint arXiv:2304.10592*, 2023. 3

A. Appendix

A.1. Visualization of More Test Cases

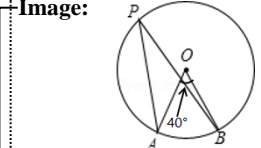
Here, we show more inference results of the basic foundation models in Figure 7 and Figure 8. Both cases show that directly solving the problem can lead to errors in the processing of visual information, even when the images are frustratingly simple. Using multimodal models to interpret images to obtain accurate fine-grained information extraction and then perform linguistic reasoning can improve the accuracy of the answer.

A.2. Used Prompt

For the compared methods, the test setting of lonely LVLM is zero-shot prompting, i.e., we directly instruct the LVLM to think and finally answer the question according to the image. The used prompts are shown in Figure 9.

For the test setting of decoupled reasoning, i.e., LVLM visual interpretation combined with LLM reasoning, we prompt LVLM with one in-context example because we found that prompting with an example can demonstrate the image interpretation task to LVLM better and make the output format of LVLM more stable. The prompt we use is shown in Figure 10.

Directly answer with VL model

Image: 

Question: As shown in the figure, then the degree of angle APB is ()
Choices: A:80° B:140° C:20° D:50°

→ Qwen2VL-7B

Solution: Since angle P is 40°, then angle APB is 2 times angle P, which is 80°. Therefore, the answer is A.

Image interpretation with VL model & answer with LM model

Describe the figure. → Qwen2VL-7B

Image description: In the figure, it is known that *angle AOB = 40°, and point P is on the circle*. The question is that what is the degree of angle APB. Find the correct answer from the choices: A:80° B:140° C:20° D:50°

→ Qwen2.5Math-7B

Solution: The angle subtended by a chord at the center of the circle is twice the angle subtended by the same chord at any point on the circumference. Given: - Angle AOB = 40° - Point P is on the circle We need to find the measure of angle APB. According to the property mentioned above, *angle APB is half of angle AOB because P is on the circumference of the circle*. So, we calculate: $\text{Angle APB} = \frac{1}{2} \times \text{Angle AOB} = \frac{1}{2} \times 40^\circ = 20^\circ$ Therefore, the correct answer is: \boxed{C}

Figure 7. Another case of comparing the solving results of a geometry math problem by directly answering with a VL model or first interpreting the image with a VL model and then answering with an LM model.

Directly answer with VL model

Image: 

Question: Find the circumference of the figure. Round to the nearest tenth. Choices: A:18.6 B:19.5 C:37.7 D:39.0

→ Qwen2VL-7B

Solution: The circumference of the circle is $2\pi r = 2\pi \times 6.2 \approx 38.28$. Therefore, the answer is D.

Image interpretation with VL model & answer with LM model

Describe the figure. → Qwen2VL-7B

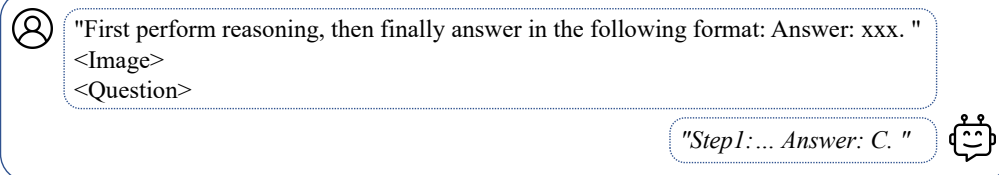
Image description: In the figure, the *diameter of the circle is 6.2 cm*. [Question] The question is that what is the circumference of the figure. Find the correct answer from the choices: A:18.6 B:19.5 C:37.7 D:39.0

→ Qwen2.5Math-7B

Solution: To find the circumference of the circle, we start with the formula for the circumference of a circle, which is given by: $C = \pi d$ where C is the circumference and d is the diameter of the circle. We are given that the diameter d is 6.2 cm. Substituting this value into the formula, we get: $C = \pi \times 6.2$ Using the approximation $\pi \approx 3.14$, we can calculate the circumference as follows: $C = 3.14 \times 6.2 = 19.52$ Now, we perform the multiplication: $C = 3.14 \times 6.2 = 19.52$ Rounding 19.52 to the nearest tenth, we get 19.5. Therefore, the circumference of the circle is: $\boxed{19.5}$ So, the correct choice is: \boxed{B}

Figure 8. Another case of comparing the solving results of a geometry math problem by directly answering with a VL model or first interpreting the image with a VL model and then answering with an LM model.

Zero-shot instruction used for problem-solving.



Zero-shot prompt used for trained LVLM image interpretation.

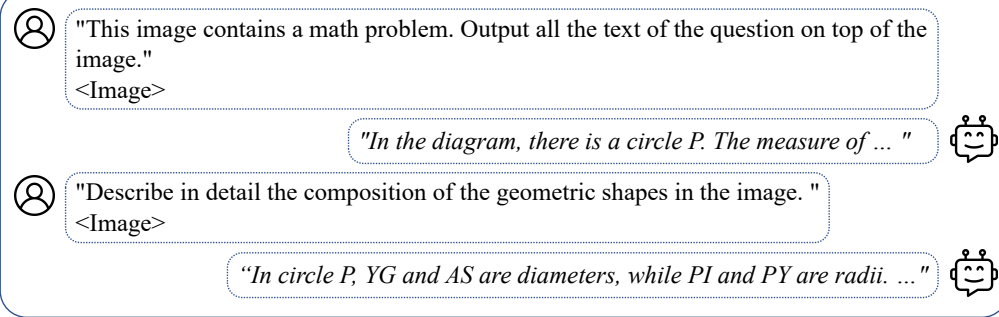


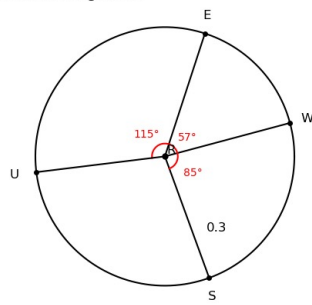
Figure 9. The zero-shot prompt used to test the base model and the trained model.



I will provide you with a geometry math problem with an image and the question. You need to summarize all the known conditions and the question (with options to choose from if available) to be answered based on the provided information and the image. Here is an example:

Problem image:

In the diagram, there is a circle R with angles SRW = 85 degrees, WRE = 57 degrees, and ERU = 115 degrees. What is the measure of angle SRU?



Question: What is the measure of angle SRU?

Summarization:

In circle R, RS, RW, RE, and RU are radii. The radius RS is 0.3 units long. The angles formed between these radii are: SRW at 85 degrees, WRE at 57 degrees, and ERU at 115 degrees.

Below is an image and description of a new geometry problem. Please give the summarized problem information according to the example above.

Problem image:

<image>

Question:

<question>

Summarization: ...



Figure 10. One-shot prompt used for image interpretation of foundation LVLM.